PCCP

Accepted manuscript version

Phys. Chem. Chem. Phys., 2017, 19, 1632-1643

DOI for the published journal article (PJA): 10.1039/c6cp04940k

Supramolecular organization of perfluorinated 1*H*-indazoles in the solid state using X-ray crystallography, SSNMR and sensitive (VCD) and non sensitive (MIR, FIR and Raman) to chirality vibrational spectroscopies†

María Mar Quesada-Moreno,[a] Juan Ramón Avilés-Moreno,[b] Juan Jesús López-González,*[a] Kane Jacob,[c,d] Laure Vendier,[c,d] Michel Etienne,*[c,d] Ibon Alkorta,[e] José Elguero[e] and Rosa Mª Claramunt[f]

[a] *Grupo de Investigación Química Física Teórica y Experimental (FQM-173), Departamento de Química Física y Analítica, Facultad de Ciencias Experimentales, Universidad de Jaén, Campus de Las Lagunillas, E-23071 Jaén, Spain. E-mail: jjlopez@ujaen.es*

[b] *Departamento de Sistemas Físicos, Químicos y Naturales, Facultad de Ciencias Experimentales, Universidad Pablo de Olavide, Carretera de Utrera Km 1, E-41013 Sevilla, Spain*

[c] *Laboratoire de Chimie de Coordination du CNRS (LCC), 205 route de Narbonne, BP 44099, 31077 Toulouse Cedex 4, France.*

[d] *Université de Toulouse, UPS, INPT, LCC, 31077 Toulouse Cedex 4, France.*

[e] *Instituto de Química Médica, CSIC, Juan de la Cierva, 3, E-28006 Madrid, Spain*

[f] *Departamento de Química Orgánica y Bio-Orgánica, Facultad de Ciencias, Universidad Nacional de Educación a Distancia, Senda del Rey, 4, E-28040 Madrid, Spain*

† Electronic supplementary information (ESI) available: Figure 1S) Molecular structures of the monomers, dimers, trimers, tetramers and pentamers of compounds **2** and **3**; Figure 2S) Experimental (top) and scaled predicted (bottom) IR spectra of compounds **2** (panel a) and **3** (panel b) in the 2000-700 cm^{-1} spectral region; Figure 3S) Experimental (top) and scaled predicted (bottom) Raman spectra of compounds **2** (panel a) and **3** (panel b) in the 2000-700 cm^{-1} spectral region; Figure 4S) Experimental and scaled predicted FarIR and Raman spectra of the monomers, dimers, trimers, tetramers and pentamers of compounds **2** (panel a) and **3** (panel b) in the solid phase (powder) in the 700-30 cm^{-1} spectral region; Figure 5S) Experimental and theoretical IR spectra (top) and experimental (top and bottom middle) and theoretical (bottom) VCD spectra of compound **2** in nujol mull in the 1215-900 cm^{-1} spectral region; Figure 6S) Experimental and theoretical IR spectra (top) and experimental (top and bottom middle) and theoretical (bottom) VCD spectra of compound **3** in nujol mull in the 1215-900 cm^{-1} spectral region; Table 1S) Comparison of experimental and calculated chemical shifts (ppm) and presence (1)/absence (0) data matrix; and Table 2S) Geometry, energy and NMR parameters for **2** and **3** calculated at B3LYP/6-311++G(d,p) computational level. Crystallographic data in CIF format, see also CCDC 1511340-1511342. See DOI: 10.1039/....

1*H*-indazole derivatives exhibit a remarkable property since some of them form chiral supramolecular structures starting from achiral monomers. The present work deals with the study of three perfluorinated 1*H*-indazoles that resolve spontaneously as conglomerates. These conglomerates can contain either a pure enantiomer (one helix) or a mixture of both enantiomers (both helices) with an enantiomeric excess (e.e.) of one of them. The difficulty of the structural analysis of this type of compounds is thus clear. We outline a complete strategy to determine the structures and configurations (*M* or *P* helices) of the enantiomers (helices) forming the conglomerates of these perfluorinated 1*H*-indazoles based on X-ray crystallography, solid state NMR spectroscopy and different solid state vibrational spectroscopies that are either sensitive (VCD) or not (FarIR, IR and Raman) to chirality, together with quantum chemical calculations (DFT).

1. Introduction

Our groups have been interested over the years in indazoles,[1,2,3,4,5] in fluorinated derivatives (generally heterocyclic)[6,7,8,9,10] and in the intersection of these two fields, the fluorinated indazoles.[11,12,13,14,15,16,17,18,19,20] The last compounds have been used in different applications, the two most significant of which are (i) as ligands in coordination chemistry (our work)[15,16,18,19] and (ii) their biological properties, particularly those of 7-fluoro-1*H*-indazole and its derivatives, that are potent and selective inhibitors of factor Xa,[21,22] as well as a norepinephrine/serotonin reuptake inhibitor for the treatment of fibromyalgia.[23] There has been some alarm about the misuse of fluoroalkylindazoles as controlled drugs.[24,25] Concerning the synthetic approaches to these products, we quote only those related to the 3-trifluoromethyl derivatives[22,26,27] and the 4,5,6,7-tetrafluoro derivatives.[22,28]

The present work concerns the perfluorinated compounds (except the NH) **1**-**3**. Our interest in these compounds is related to a remarkable property some indazoles present: upon crystallization, chiral supramolecular structures are formed from achiral monomers.

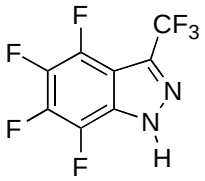

1

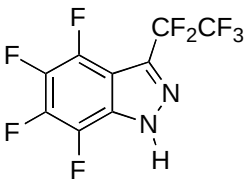

2

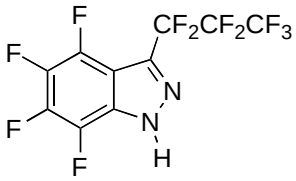

3

In the crystal, *N*-unsubstituted 1*H*-indazoles (the 2*H*-tautomers are generally much less stable)[29,30] can form three kinds of structures held together by N–H···N hydrogen bonds (Scheme 1). Most *N*-unsubstituted 1*H*-indazoles lack stereogenic centres, either intrinsically, like in indazole itself (R = R' = H), or statistically by fast rotation of alkyl chains about the C-C bonds.

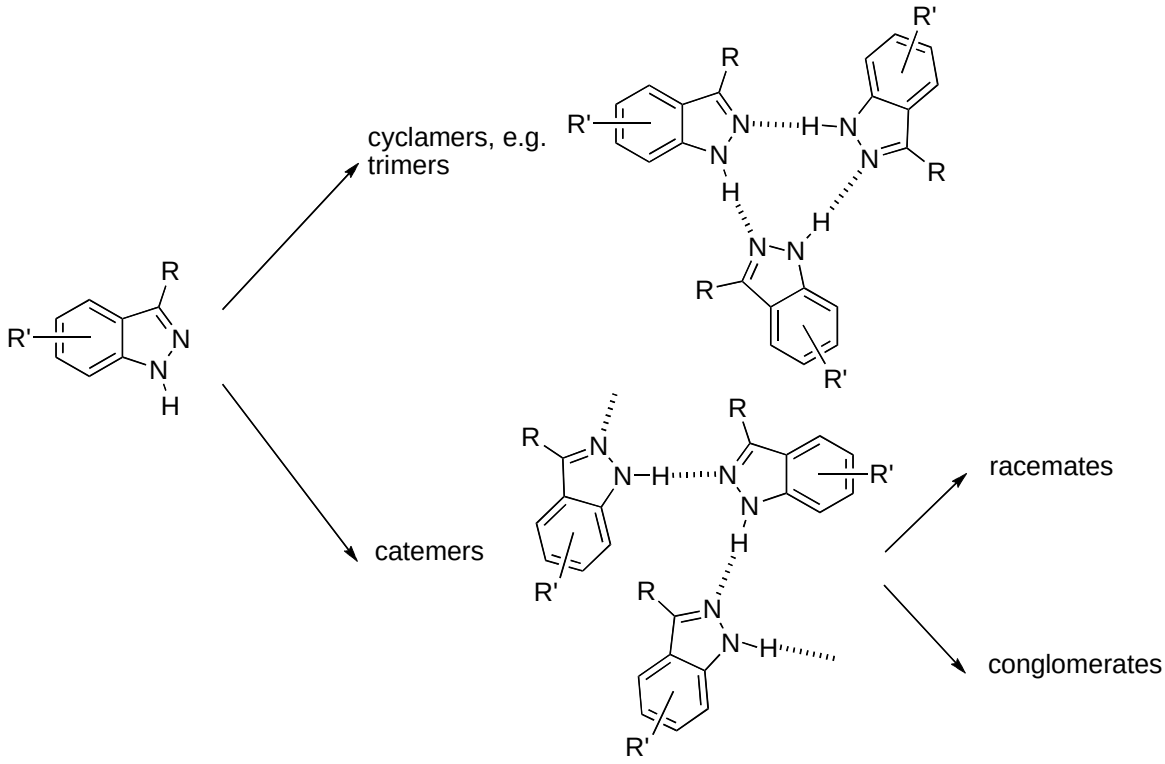

Scheme 1 Structures found in 1*H*-indazole crystals.

They can form cyclic structures, cyclamers, the most common being the trimers that are devoid of chirality. They can also form chains, catemers, of helical chirality (*M* or *P*).[31] Usually, both enantiomeric chains are found in the crystal – racemates –, but in some cases, the crystal contains only one chain – conglomerates –[32] (ideally, there should be a 50:50 mixture of both types of crystals, but this situation is never found in a single crystallization experiment). When a compound crystallizes as a conglomerate (spontaneous resolution), it often means that the compound crystallizes as a catemer in which only one enantiomer is present in the unit cell for a given crystal that can be separated manually.[32] The last case is what interests us here. Moreover, spontaneous resolution of achiral molecules has become a very relevant topic because it is related to the origins of life.[4,32,33,34,35,36,37]. Recall that although *M* and *P* enantiomers have the same probability to be formed, a 50:50 mixture of crystals is never formed;[38] due to ripening processes related to the different size of the crystals, an enantiomer always predominates in each crystallization experiment. As the number of crystallizations becomes very large the ratio of the two enantiomers becomes close to one.

Note that other NH-azoles devoid of stereogenic centres also crystallize forming conglomerates although this phenomenon remains rare: pyrazoles (3,5-dimethyl-4-nitro-1*H*-pyrazole, space group $P3_121$),[33] benzimidazoles (2-propyl-1*H*-benzimidazole, space group $P2_12_12_1$)[39] and benzotriazoles (1*H*-benzotriazole, space group $P2_1$).[40] Amongst the conglomerates of NH-indazoles, we have already studied 1*H*-indazole itself (space group $P2_1$)[34] and 3-trifluoromethyl-4,5,6,7-tetrafluoro-1*H*-indazole (**1**) (space group $P3_2$).[4] The latter will be considered here only for comparative purposes.

In this work, we have followed a unified strategy to study the supramolecular organization of two new conglomerates – namely, 3-(perfluoroethyl)-4,5,6,7-tetrafluoro-1*H*-indazole (**2**, CSD code YODJIM)[4,11] and 3-(perfluoropropyl)-4,5,6,7-tetrafluoro-1*H*-indazole (**3**, YODJOS)[19] – using (i) X-ray crystallography (new data sets), (ii) solid state multinuclear NMR spectroscopy, (iii) different vibrational spectroscopies that are either sensitive (Vibrational Circular Dichroism, VCD) or not (IR, FIR and Raman) to chirality, and (iv) quantum chemical calculations. We will use the numbers **1**, **2** and **3** for the compounds, irresponsibly of their physical state, and LIDGEL, YODJOS and YODJIM, for their corresponding crystal structures.

Herein, we report the *P* and *M* absolute configurations of each catemer forming conglomerates corresponding to the crystals of compounds **2** and **3**. When the crystals are obtained by repeated sublimations under static vacuum at constant temperature, the same enantiomer is formed for these compounds, the *M* helix for compound **2** and the *P* helix for **3**. However, when the crystals are recrystallized in acetone by removing the solvent using a magnetic stirrer and a N_2 flow, the enantiomeric structures for both compounds are observed, that is, the *P* helix for compound **2** and the *M* helix for compound **3**. For an unambiguous determination of the absolute configuration quantum chemical calculations were accomplished, getting the best reproduction with a pentamer model. It is suggested that a better agreement between the experimental and theoretical VCD spectra would be achieved by a better simulation of the *P* or *M* helix models with the calculation of higher-molecular-weight oligomers structures than the pentamers. We show that solid-state NMR (SSNMR), IR, Raman and VCD spectroscopies provide a complete characterization of this kind of conglomerates. The helicities of selected single crystals of **2** and **3** have also been obtained from new X-ray diffraction data sets.

2. Experimental

2.1. Synthesis

Compounds **2** and **3** were synthesized according to published procedures.[11,19] The crystals used in this study were obtained, on the one hand, by repeated sublimations under static vacuum (*ca.* 8×10^{-2} mbar) at a temperature of 70 °C and, on the other, by recrystallizing these crystals in acetone by

removing the solvent using a magnetic stirrer and a N_2 flow. We also recrystallized both compounds in acetone without using the magnetic stirrer and the N_2 flow.

2.2. SSNMR

Solid state NMR spectra were recorded on a WB 400 (9.4 Tesla, 400.60 MHz for ^{1}H, 100.73 MHz for ^{13}C and 40.60 MHz for ^{15}N) at 300 K using a 4 mm DVT probe head. Samples were carefully packed in a 4-mm diameter cylindrical zirconia rotor with Kel-F end-caps. Operating conditions involved 2.9 μs 90° ^{1}H pulses and decoupling field strength of 86.2 kHz by SPINAL 64 sequence. ^{13}C spectra were originally referenced to a glycine sample and then the chemical shifts were recalculated to the Me_4Si (for the carbonyl atom δ (glycine) = 176.1 ppm) and ^{15}N spectra to $^{15}NH_4Cl$ and then converted to nitromethane scale using the relationship: δ ^{15}N (nitromethane) = δ ^{15}N (ammonium chloride) – 338.1 ppm. In order to distinguish protonated and unprotonated carbon and nitrogen atoms, the NQS (Non-Quaternary Suppression) experiment by conventional cross-polarization was recorded; before the acquisition the decoupler is switched off for a very short time of 25 μs for ^{13}C and 80 μs for ^{15}N.[41,42,43]

^{19}F (376.94 MHz) NMR spectra have been obtained on a Bruker WB 400 spectrometer using a MAS DVT BL2.5 X/F/H double resonance probe head. Samples were carefully packed in 2.5 mm diameter cylindrical zirconia rotors with Kel-F end-caps. Samples were spun at the magic angle at rates of 25 kHz and the experiments were carried out at ambient probe temperature. The ^{19}F spectra were referenced to an ammonium trifluoroacetate sample and then the chemical shifts were recalculated to the $CFCl_3$ ($\delta(CF_3COO^-NH_4^+)$ = –72.0 ppm)

2.3. FarIR, MIR, Raman and VCD

The IR spectra of the two compounds in solid phase (powder) were recorded using a Bruker Vertex 70 in the 2000-30 cm^{-1} region, with 100-200 scans and resolutions of 2 cm^{-1} (FarIR) and 4 cm^{-1} (MIR) for compound **2** and 4 cm^{-1} (FarIR) and 1 cm^{-1} (MIR) for compound **3**. The Pt ATR accessory (single reflection diamond ATR accessory) and the silicon beam-splitter were used for the Far-IR region.

The Raman spectra were recorded on a MultiRAM Stand-Alone FT-Raman spectrometer that was equipped with an Nd:YAG laser (excitation line: 1064 nm) and a Ge detector that was cooled to liquid-nitrogen temperature. The spectra were measured using a standard solid support (resolution: 2 cm^{-1}, scans: 200-300) in the 2000-100 cm^{-1} region.

The IR and VCD spectra of crystals, obtained by both ways described in section 2.1, of compounds **2** and **3** in nujol mull were recorded on a JASCO FVS-4000 FTIR spectrometer that was equipped with an MCTV (2000-900 cm^{-1}) detector. A few milligrams of **2** and **3** were mixed with nujol mineral oil to obtain suitable mulls. Special attention is required when working with solid samples for CD spectroscopy.[44,45,46] We measured the mulls at several positions by rotating the sample around both the beam-propagation axes (90º and 180º, face A) and that perpendicular to it (180º, face B) to obtain the "true" VCD peaks and ascertain the absence of artefacts in the VCD spectra.[45,46] All of the spectra were recorded using a standard cell that was equipped with KBr and BaF_2 windows (resolution: 4 cm^{-1}; scans: 2000-8000, in blocks of 2000 scans). For the baseline correction, we subtracted the nujol signals from the raw VCD spectra of both compounds. Later, for each compound, we averaged these (nujol corrected) VCD spectra of the pair of enantiomers obtaining the VCD baseline, which was subtracted from them giving the baseline corrected VCD spectra.

We tried to record the VCD spectra of several large single crystals emulsified in nujol mull, but the corresponding VCD spectra were of low quality (less intense). For this reason, we recorded the VCD spectra of several single crystals mixed and emulsified in nujol mull. The spectra were of high quality (more intense) but similar to those of individual single crystals.

2.4. Computational details

We have carried out two different kinds of calculations, both with the hybrid HF/DFT B3LYP computational method. Those calculations corresponding to IR, Raman and VCD at the B3LYP/6-31G(d) level.[47] In this case, fragments of the X-ray geometry were used for the catemers (dimer to pentamer) and only the position of the NH proton was optimized. Although these structures are not minima, we carried out frequency calculations.

For the monomers of the NMR part we used the B3LYP/6-311++G(d,p) level.[48] In this case, frequency calculations were carried out to verify that the structures obtained correspond to energetic minima. These geometries have been used for the calculation of the absolute chemical shieldings with the GIAO method.[49,50]

All the calculations have been carried out with the Gaussian-09 package.[51]

Equations 18-20 have been used to transform absolute shieldings into chemical shifts:

$\delta^{1}H = 31.0 - 0.97*\sigma^{1}H$, (reference TMS, 0.00 ppm) (Eq. 18)[52]
$\delta^{13}C = 175.7 - 0.963*\sigma^{13}C$, (reference TMS, 0.00 ppm) (Eq. 19)[53]
$\delta^{15}N = -152.0 - 0.946*\sigma^{15}N$, (reference TMS, 0.00 ppm) (Eq. 19)[53]
$\delta^{19}F = 162.1 - 0.959*\sigma^{19}F$, (reference $CFCl_3$, 0.00 ppm) (Eq. 20)[54]

2.5 X-ray crystallography.

Crystals of **2** were cut from long (*ca* 3 cm) and thick crystal (*ca* 0.6 mm) obtained by slow sublimation under static vacuum. Two single crystals were analysed. Crystals of **3** were obtained as small needles from sublimation under static vacuum. Data for **2 (CCDC 1511341)** were collected at low temperature (110 K) on a Gemini Agilent diffractometer using a graphite-monochromated Cu-Kα Enhance radiation (λ = 1.54184 Å) and equipped with an Oxford Instrument Cooler Device. The geometry of the Gemini diffractometer does not allow to reach a value of sinθ/λ to at least 0.6; in the present case sinθ/λ = 0.5709. Data of **2 (CCDC 1511342)** and **3 (CCDC 1511340)** were collected at low temperature (100 K) on a Bruker Kappa Photon diffractometer using a micro-focus Cu-Kα radiation (λ = 1.54184 Å) and equipped with an Oxford Cryosystems Cryostream Cooler Device. The final unit cell parameters have been obtained by means of a least-squares refinement. The structures have been solved by direct methods using SIR92,[55] and refined by means of least-squares procedures on a F^2 with the aid of the program SHELXL[56] included in the softwares package WinGX[57] version 1.63 or with the program CRYSTALS.[58] The Atomic Scattering Factors were taken from International tables for X-Ray Crystallography.[59] The hydrogen atoms were located by Fourier differences and isotropically refined by using a riding model. Crystal and refinement data are collected in Table 1 and the analysis of the absolute structure using Flack[60] and Hooft[61] parameters is found in Table 2.

3. Results and discussion

Our strategy for the study of **2** and **3** in solid phase has been: 1) to record the NMR spectra of the two compounds and to analyse them with the corresponding calculations; 2) to record their IR (including FIR) and Raman spectra; 3) to compare these spectra with those calculated for monomers and oligomers at the B3LYP/6-31G(d) level of theory; 4) to record the IR and VCD spectra in nujol mull; 5) to compare their experimental VCD spectra with those calculated for oligomers at the same level of theory as above. The main goal is to associate the experimental VCD spectra with a given chiral supramolecular structure. For this purpose, a previous NMR-IR-Raman analyses and an adequate correction of the baseline of the VCD spectra (see 2.3. section) together with accurate calculations are crucial for a correct VCD assignment. The determination of the

absolute structure of selected single crystals of **2** and **3** by X-ray diffraction analysis is also provided.

Given our own experience, the interpretation of complex VCD features is facilitated by a prior vibrational analysis based on IR and Raman spectra and quantum chemical calculations.[4,34] When the chirality appears in the secondary structure, it is mandatory to calculate catemers with an increasing number of monomers until the experiment becomes acceptably reproduced.[4,34]

3.1. Crystallography

The X-ray crystal structures of the three indazoles **1-3** have been previously recorded.[11,19] The three compounds crystallize as conglomerates. Compounds **1** and **2** crystallize in the space group $P3_2$ forming helices of order 3 while compound **3** (space group $P2_12_12_1$) forms a helical catemer of order 2. The diffraction data used MoKα radiation. In the absence of heavy atom, anomalous diffusion does not differentiate Friedel pairs and the absolute configurations of the helices cannot be determined. New data sets have now been collected with CuKα radiation for indazoles **2** and **3** (Table 1) with the goal of obtaining the absolute configuration of the helices. The analysis of the absolute structure is provided in Table 2.

Two data sets were collected for **2**; both of them confirmed the overall structure recorded previously (YODJIM).[11] A long (*ca* 3 cm) and thick crystal (*ca* 0.6 mm) of **2** was carefully cut and two single crystals were analysed. For one of them (CCDC 1511341), the data were collected at 110 K on a diffractometer operating with a normal Cu electrode. Refinement of the structure yielded a Flack parameter of -0.14(16) and the statistical analysis[33] that follows the computation of the Hooft parameter supports an *M* helix as the absolute structure (Fig. 1). The data set for the second crystal (CCDC 1511342) was obtained from a Cu microsource. While the structure determination and refinement proceeded smoothly, a twinning by inversion was established from the analysis of the Flack and Hooft parameters (Table 2). Both *M* and *P* helices are present. This confirms that both enantiomers can be formed upon sublimation. The crystal structure of **3** with the Cu microsource (Table 1-2) yielded a single enantiomer with an *M* configuration (Fig. 1). The rest of the structure is fully similar to that obtained previously with MoKα radiation (YODJOS).[19]

Table 1. Crystal data and refinement parameters for indazoles **2-3** (R' = 4,5,6,7-tetrafluoro).

Compound	**2**	**2**	**3**
CCDC number	1511341	1511342	1511340
R	CF_2CF_3	CF_2CF_3	$CF_2CF_2CF_3$
Formula	$C_9HF_9N_2$	$C_9HF_9N_2$	$C_{10}HF_{11}N_2$
Radiation	CuKα	CuKα	CuKα
Size/ mm	0.2 x 0.03 x 0.02	0.10 x 0.20 x 0.25	
Wavelength λ/ Å	1.54184	1.54180	1.54178
Crystal system	Trigonal	Trigonal	Orthorhombic
Space group	$P3_2$	$P3_2$	$P2_12_12_1$
a/ Å	12.4065(3)	12.3863(7)	5.1207(5)
b/ Å	12.4065(3)	12.3863(7)	9.1029(8)
c/ Å	5.5725(2)	5.5727(3)	24.816(2)
V/ Å^3	742.81(4)	740.42(7)	1156.75(18)
Z (*Z'*)	3 (1)	3 (1)	4 (1)

T/ K	110	100	100
Data/restraints/parameters	1554 [777] / 1 / 185	1952 [976] / 1 / 182	2298 [1378] / 0 / 209
Final R indices ($I>2\sigma(I)$)	R1 = 0.0238 wR2 = 0.0606	R1 = 0.0276 wR2 = 0.0688	R1 = 0.0625 wR2 = 0.1542
Largest diff. peak / hole/ e.Å^{-3}	0.153 / -0.175	0.24 / -0.26	0.544 / -0.378

Table 2. Absolute structures for crystals of **2** and **3**.

Compound	Flack parameter	Hooft parameter	p2(correct)	p3(correct)	p3(twin)	p3(inverse)
2 (CCDC 1511341)	-0.14(16)	-0.16(12)	1.000	1.000	0.000	0.000
2 (CCDC 1511342)	0.22(10)	0.23(4)	-	0.978	0.022	0.000
3 (CCDC 1511340)	0.1 (4)	0.07(17)	1.000	0.955	0.045	0.000

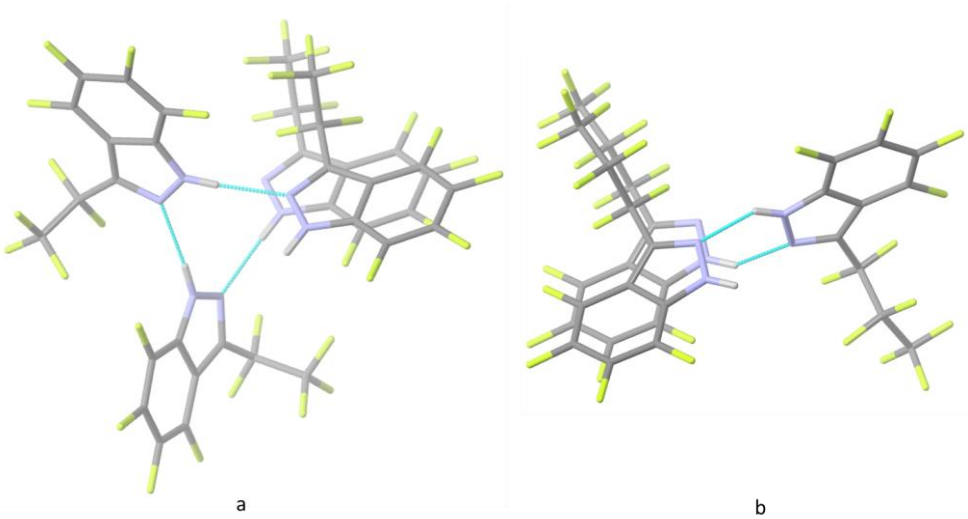

Fig. 1. The absolute structures (*M* helices) of indazole **2** (a) and **3** (b) as determined by X-ray diffraction.

We have optimized the geometries of the three indazoles at the B3LYP/6-311++G(d,p) level in the gas phase. They are very close to the experimental ones, particularly with respect to the conformation of the perfluoroethyl and perfluoropropyl chains (Fig. 2).

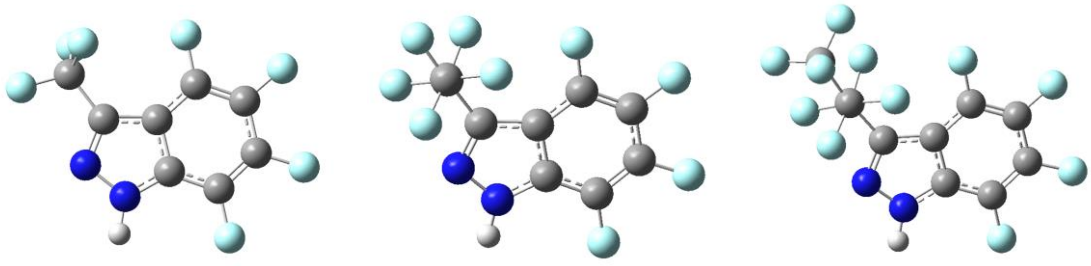

Fig. 2. The optimized structures of indazoles **1**, **2** and **3**.

3.2. SSNMR results

Table 3 contains all the available information, both experimental and calculated, on indazoles **1-3**.

Table 3 ^{13}C, ^{15}N and ^{19}F chemical shifts (δ, ppm) of compounds **1-3**. The experimental values correspond to SSNMR while the calculated ones correspond to isolated molecules in the gas phase.

^{13}C

Compound	C3	C3a	C4	C5	C6	C7	C7a	3R
1, CF_3 [11]	136.2	106.3	139*	139*	139*	133*	128.1	120*
GIAO	136.8	108.1	142.0	139.9	143.4	135.0	127.2	124.9
2, C_2F_5	129.3	108.1	133.7	133.7	133.7	129.3	129.3	108.1 (CF_2), 129.3 (CF_3)
GIAO	136.2	109.2	142.2	140.2	143.3	133.9	127.0	114.0 (CF_2), 123.4 (CF_3)
3, C_3F_7	134.0	108.4	134.0	134.0	134.0	127.8	127.8	109.7 (CF_2 α), 108.4 (CF_2 β), 127.8 (CF_3)
GIAO	135.9	109.8	141.4	140.1	143.0	134.1	126.7	116.4 (CF_2 α), 112.5 (CF_2 β), 122.6 (CF_3)

* very broad.

^{15}N

Compound	N1H	N2
1, CF_3 [11]	–200.0	–81.9
GIAO	–216.9	–60.9
2, C_2F_5	–195.6	–76.9
GIAO	–213.4	–56.2
3, C_3F_7	–195.9	–71.6
GIAO	–213.0	–55.8

^{19}F

Compound	F4	F5	F6	F7	3R
1, CF_3 [11]	–141.2	–160.5	–154.5	–156.7	–62.7 (CF_3)
GIAO	–136.7	–159.9	–151.4	–161.9	–60.8 (CF_3, mean)
2, C_2F_5	–138.6	–155.7	–151.9	–159.4	–111.5, –118.4 (CF_2 α), –84.2 (CF_3)
GIAO	–134.1	–159.4	–151.9	–161.6	–109.3 (α1F, CF_2), –116.0 (α2F, CF_2), –84.1 (CF_3, mean)
3, C_3F_7	–137.9	–162.3	–155.7	–157.6	–111.7, –113.8 (CF_2 α), –123.9 (CF_2 β), –79.4 (CF_3)
GIAO					–107.7 (α1F, CF_2), –111.0 (α2F, CF_2), –123.4, –123.8 (CF_2 β), –78.4 (CF_3, mean)

Note that because of the absence of free rotation in the solid state, the α fluorine atoms are diastereotopic as expected from the X-ray structures (Fig. 3). The β fluorine atoms of **3** are also diastereotopic but their anisochrony is too small to be resolved in SSNMR.

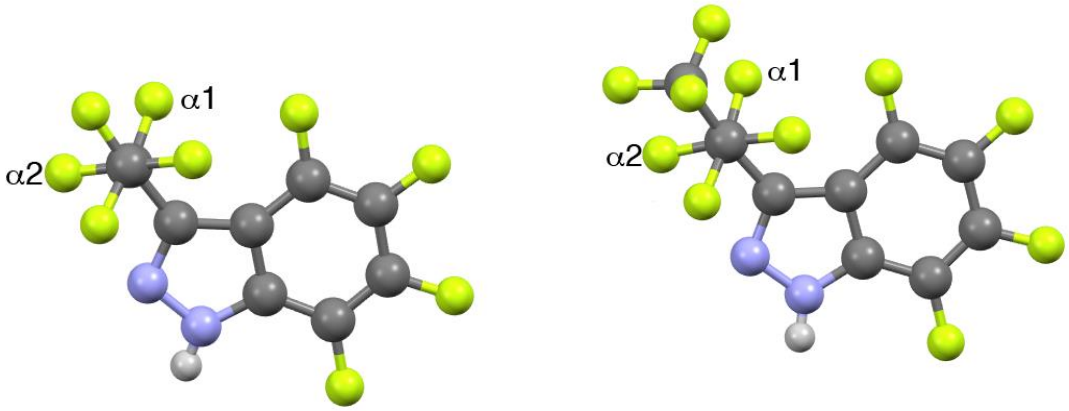

2 **3**

Fig. 3 The X-ray structures of compounds **2** and **3**.

It might be argued that comparing NMR data obtained in the solid state (CPMAS and MAS techniques) with calculated values corresponding to isolated molecules in the gas phase could appear crude but with only two dummies for the N–H···N hydrogen-bonded N atoms, the results are highly satisfying:

Exp. (ppm) = –(2.1±0.6) + (0.990±0.004) – (17.7±2.1) N2 + (17.2±2.3) N1H, n = 49, R^2 = 0.999, RMS = 3.5 ppm

As expected, the N–H···N hydrogen bonds present in the crystal structures affect both ^{15}N signals in opposite ways. A plot of experimental *versus* fitted values (see Fig. 4) shows the excellent linear agreement.

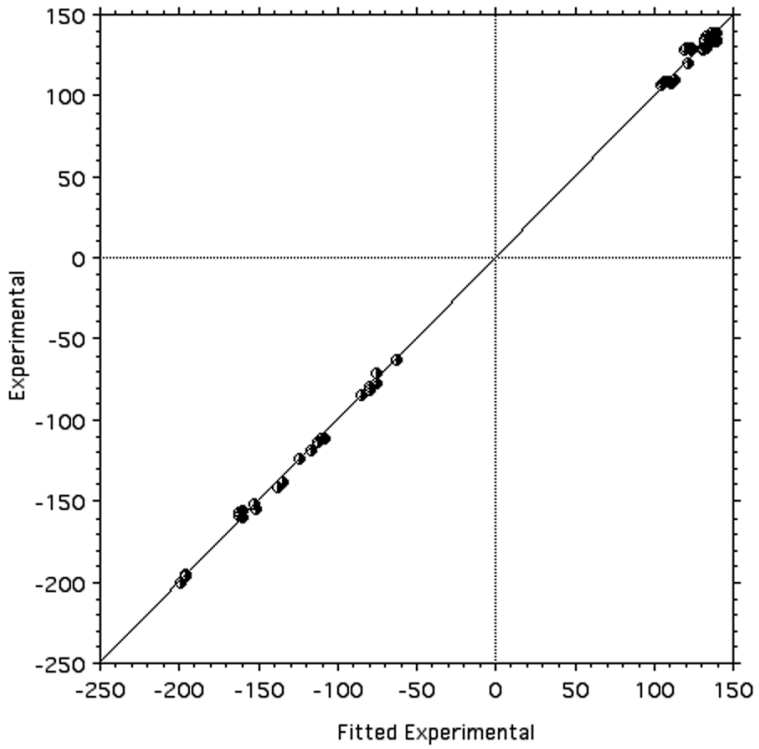

Fig. 4 Plot of experimental *vs.* fitted values for 49 points including ^{13}C, ^{15}N and ^{19}F chemical shifts.

This section dealing with SSNMR results, although insensitive to chirality, proves that the bulk samples that will be used for vibrational spectroscopy behave like the single crystals used for X-ray, in particular in what concerns the conformation of the perfluoroalkyl chains. Moreover, the minimum energy geometries calculated theoretically predict well the chemical shifts measured in the solid state; therefore, they can be used to build up the catemers as required for the discussion of the vibrational results.

3.3. Nonchiroptical Vibrational Spectroscopies (FIR, IR and Raman)

We first focused our attention on the intermediate and far regions (2000-30 cm^{-1}) of the vibrational spectra of **2** and **3** (see Fig. 5 and Supporting Information). In the intermediate region (2000-700 cm^{-1}), there are many bands that could be reproduced by the theoretical spectra of the monomers of compounds **2** and **3**, but the theoretical spectra of the oligomers achieve a better agreement by reproducing some bands that are absent in the theoretical spectra of the monomers. Consider for example the bands appearing in the 800-700 cm^{-1} region in both the IR and Raman spectra of the two compounds, which are associated with N-H waggings, in plane ring deformations and symmetric bendings of CF_3 groups. In Figure 1S of ref. 4 it can be seen that a similar situation occurs for compound **1**. Note that DFT calculations have been performed in the harmonic approximation which does not take into account overtones and combination bands. Consequently, some bands appearing in the recorded IR and Raman spectra are not predicted here.

In the low frequency region (Fig 5), bands corresponding to normal modes with contributions from wagging, rocking and torsion modes are present. Thus, the region below 700 cm^{-1} is very useful for distinguishing among different structures of compounds **2** (Fig 5a) and **3** (Fig 5b). Figs. 5a and 4S in SI show some examples of these modes, such as the bands at 603 cm^{-1} (IR and Raman spectra), 484 cm^{-1} (IR and Raman spectra), 446 cm^{-1} (IR, 444 cm^{-1} in Raman spectrum) and 431 cm^{-1} (IR, 428 cm^{-1} in Raman spectrum), which are assigned to complex deformation and torsion motions as in plane/out plane ring deformations and N-H waggings involving two or more hydrogen bonded monomer subunits. These four bands are due to the presence of oligomers, that is, they are predicted to have a different intensity or to be absent in the monomer model. Similar conclusions are valid for **3** in Fig. 5b. A pentamer model predicts significantly better the experimental bands at 611 cm^{-1} (IR, 606 cm^{-1} in Raman spectrum), 566 cm^{-1} (IR, 571 cm^{-1} in Raman spectrum) and 487 cm^{-1} (IR and Raman spectra).

Finally, it must be emphasized that the monomers of **2** and **3** do not present any band below 160 cm^{-1}. Accordingly, oligomers must be present in these crystals. Particularly noteworthy are the five bands observed at 157 cm^{-1} (FarIR, 155 cm^{-1} in Raman spectrum), 136 cm^{-1} (FarIR, 134 cm^{-1} in Raman spectrum), 120 cm^{-1} (Raman), 83 cm^{-1} (FarIR) and 56 cm^{-1} (FarIR) in the FarIR and Raman spectra of solid **2,** as well as the four bands appearing at 148 cm^{-1} (FarIR and Raman), 129 cm^{-1} (FarIR and Raman), 117 cm^{-1} (FarIR and Raman) and 64 cm^{-1} (FarIR) in the spectra of solid **3** that are assigned to torsion normal modes of one subunit of **2** or **3** with respect to the others. Note that in the case of crystals of **1**,[4] this low-frequency region was also very helpful to prove the presence of oligomers.

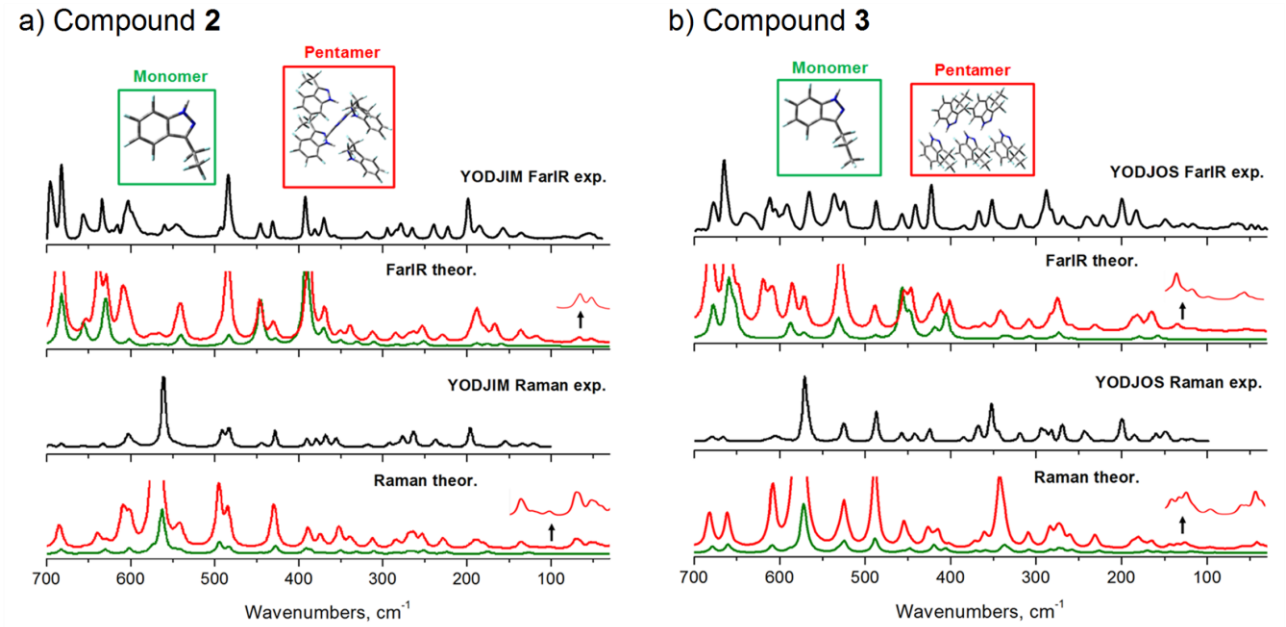

Fig. 5 Experimental and predicted FarIR and Raman spectra (scaled) of (a) compound **2** and (b) compound **3** in the solid phase (powder) in the 700-30 cm^{-1} spectral region. Scaling frequency factor of 0.99.[62] Lorentzian function, pitch = 1 cm^{-1}, FWHM (Full Width Half Maximum) = 4 cm^{-1}

3.4. Chiroptical Vibrational Spectroscopy (VCD)

So far, we have analysed the FarIR, MIR and Raman spectra considering the monomer and the oligomers species of compounds **2** and **3**; although the larger oligomers structures improved their analysis. The next step was to shed light on the possible chirality and, then, absolute configuration of catemers of **2** and **3** in the solid state. Indeed, despite of the achirality of their corresponding monomers in gas phase or liquid solutions, supramolecular chirality is present in their crystals and *M* or *P* helix models could predominate in them (enantiomeric excess). For this, we used the VCD technique, which is sensitive to chirality, combined with theoretical calculations. The signs of the rotatory strength (signs of the VCD bands) were required for the determination of the absolute configuration of the catemers.[63,64,65]

Figs. 6 and 7 show the theoretical and experimental IR and VCD spectra in nujol mull for both enantiomers of compounds **2** and **3**, respectively. The bottom graphs depict the predicted scaled VCD spectra of the pentamers of **2** and **3**, in which the *M* helix model has been marked in red colour and the *P* helix model in blue colour.

We observe a fair agreement between the experimental VCD spectra of crystals of **2** and **3** and the predicted scaled of the corresponding *M* helix oligomers and *P* helix oligomers. In the crystals of compounds **2** and **3**, a few key experimental VCD bands demonstrate the predominance of one of the two proposed helix models, as indicated above. The literature contains examples about how the assignments were made in similar situations.[4,34,66] The main conclusions are:

(1) For the red VCD spectrum of compound **2** catemer, the three (+, +, –) bands at 1075 cm^{-1} (VCD, 1078 cm^{-1} in IR and 1080 cm^{-1} in Raman spectrum), 1036 cm^{-1} (VCD, IR and Raman) and 986 cm^{-1} (VCD, 989 cm^{-1} in IR, 991 cm^{-1} in Raman spectrum) and the (+, –) couplet at 941 cm^{-1} and 933 cm^{-1} (VCD, 939 cm^{-1} in the IR and Raman spectra) are the signature of a *M* helix, confirming that in the crystal **2** organizes itself as a left-handed helix when it is obtained by repeated sublimations.

(2) The situation in the blue VCD spectrum of catemer **3** is quite different when it is obtained in the same way (repeated sublimations). In this case, the chiroptical features point to the existence of a right-handed *P* helix. The (–, –, –, –) bands at 1124 cm^{-1} (VCD, 1119 cm^{-1} in IR and Raman), 1065 cm^{-1} (VCD, 1062 cm^{-1} in IR and Raman spectra), 1026 cm^{-1} (VCD, IR and

Raman spectra) and 961 cm^{-1} (VCD, 958 cm^{-1} in IR and Raman) allow us to assign unambiguously the *P* helix to the supramolecular structure of **3**.

To sum up, the best agreement between experimental and theoretical spectra has been reached in both cases with the oligomers of larger size, *i.e.*, pentamers (see Figs. 5S and 6S in SI); the signs of the VCD bands confirm the existence of a *M* helix in the case of compound **2** and a *P* helix for compound **3**, when the crystals studied for both compounds were those obtained directly by sublimation. Different helicities are observed upon changing the experimental conditions. The absolute configuration was the opposite when the crystals were obtained from acetone by removing the solvent using a magnetic stirrer under a N_2 flow. Recrystallization from acetone without stirring and the N_2 flow provided crystals with the same absolute configuration as that obtained from sublimed samples. For compound **1**, the best agreement was achieved by the tetramer model (the largest modelled oligomer), and the signs of the rotatory strength pointed the existence of a *P* helix.[4]

Fig. 8 shows a superposition of the VCD spectra corresponding to the *P* (top) and *M* (bottom) helices of compounds **2** and **3** highlighting the spectral differences between them. To analyse some of these spectral differences, we focus our attention on the VCD spectra of *M* helix (bottom graphic). In both compounds, there is a (+, –) couplet with the same signs but different positions according to the compound. This couplet appears at 941 cm^{-1} and 933 cm^{-1} in compound **2** and at 961 cm^{-1} and 954 cm^{-1} in compound **3**. The same occurs for the (+) band at 1036 cm^{-1} (compound **2**) and 1026 cm^{-1} (compound **3**). There is a band with similar position but different sign according to the compound; it appears with negative sign at 1132 cm^{-1} for compound **2** and at 1124 cm^{-1} with positive sign for compound **3**. It is surprising how the difference in the length of the side chain in the monomer can dramatically change the spectral features of their supramolecular structures, *i.e.* the catemers. The space groups determined by X-ray[4,11,19] are $P3_2$ and $P2_12_12_1$ for compounds **2** and **3**, respectively. It is important to bear in mind that the quantum chemical calculations were carried out starting from these X-ray data (see 2.3 section "Computational details").

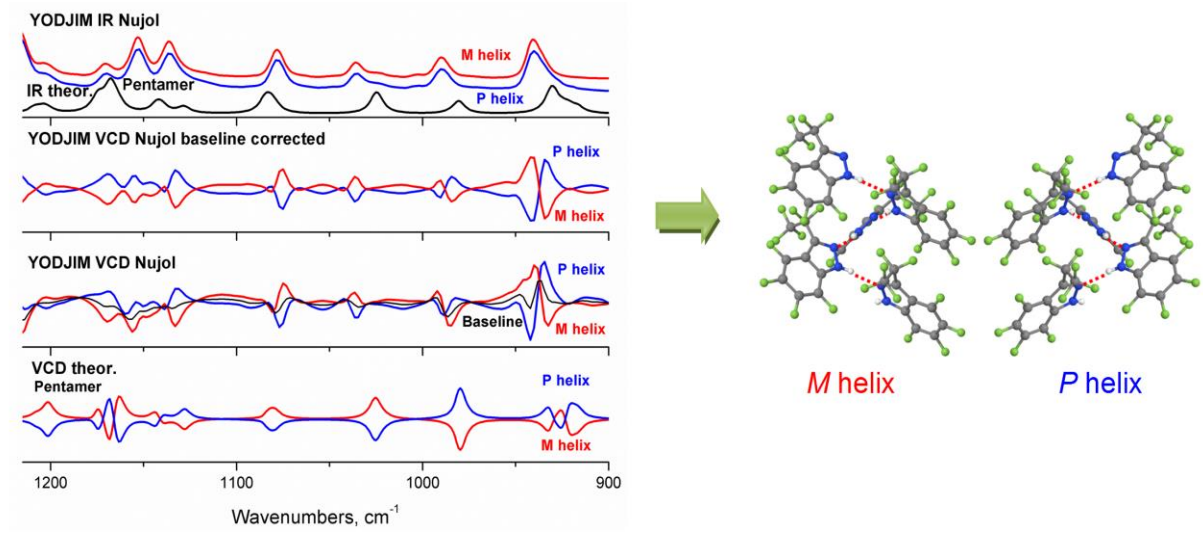

Fig. 6 Experimental and theoretical IR spectra (top) and experimental (top and bottom middle) and theoretical (bottom) VCD spectra of compound **2** in nujol mull in the 1215-900 cm^{-1} spectral region. In the bottom middle graphic, the raw VCD spectra were corrected by subtracting nujol signals. The average of these two VCD spectra provides the baseline, which was subtracted from them giving the baseline corrected VCD spectra shown in the top middle graphic. Scaling frequency factor of 0.96.[62] Lorentzian function, pitch = 1 cm^{-1}, FWHM (Full Width Half Maximum) = 4 cm^{-1}

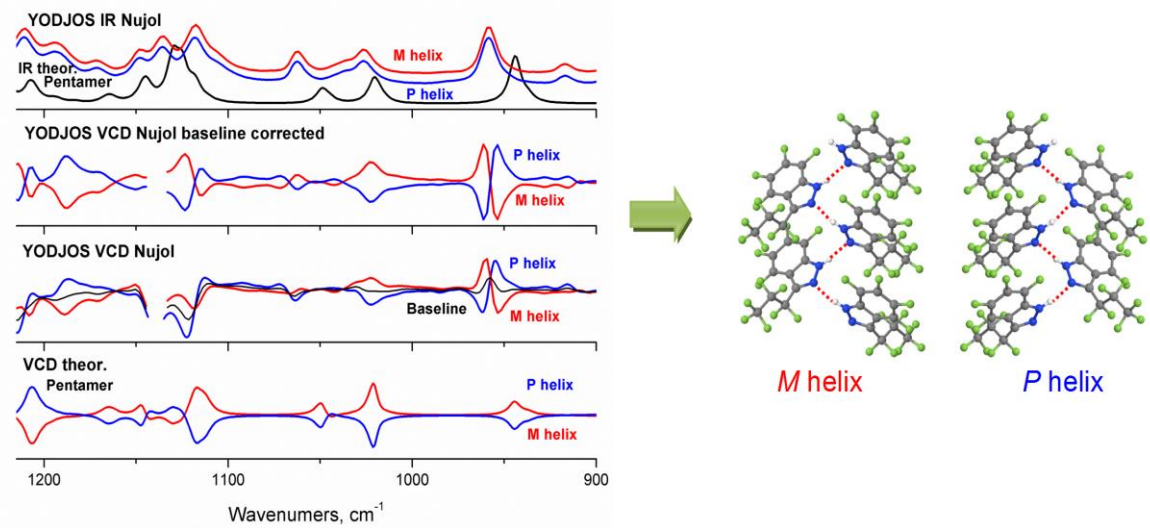

Fig. 7 Experimental and theoretical IR spectra (top) and experimental (top and bottom middle) and theoretical (bottom) VCD spectra of compound **3** in nujol mull in the 1215-900 cm^{-1} spectral region. In the bottom middle graphic, the raw VCD spectra were corrected by subtracting nujol signals. The average of these two VCD spectra provides the baseline, which was subtracted from them giving the baseline corrected VCD spectra shown in the top middle graphic. Scaling frequency factor of 0.96.[62] Lorentzian function, pitch = 1 cm^{-1}, FWHM (Full Width Half Maximum) = 4 cm^{-1}

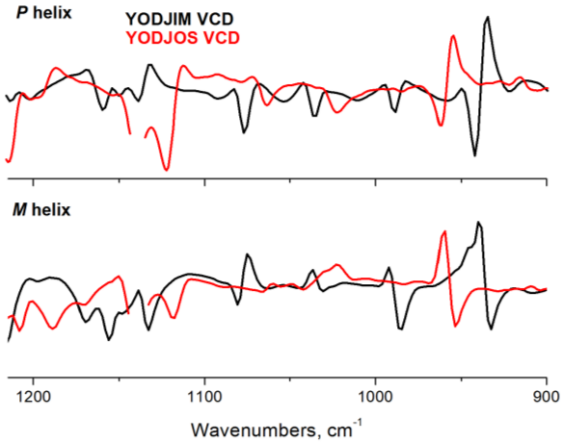

Fig. 8 Comparison of the nujol corrected experimental VCD spectra obtained for *P* (top) and *M* (bottom) helices for compounds **2** (in black) and **3** (in red), in nujol mull in the 1215-900 cm^{-1} spectral region.

4. Conclusions

i) Polycrystalline samples of **2** and **3** have been studied in detail by a combination of X-ray crystallography, solid state NMR techniques, non sensitive (IR and Raman) and sensitive (VCD) to chirality vibrational spectroscopies, and quantum chemical calculations. The analysis of low-frequency region (700-30 cm^{-1}) in the FarIR and Raman spectra deserves a special mention since it has been of valuable importance to determine the presence of catemers in the crystals of compounds **2** and **3**. After a detailed analysis of their VCD spectra, we concluded that the configurations of the catemers corresponding to compounds **2** and **3** were *M* and *P* helices, respectively, when the crystals were obtained by repeated sublimations, and the opposite *P* and *M* helices when a recrystallization in acetone by removing the solvent using a magnetic stirrer and a N_2 flow was used. Although dimer, trimer, tetramer and pentamer models predicted adequately the experimental FarIR, MIR, Raman and VCD spectra of crystals of **2** and **3**, the pentamer model improved the agreement significantly. With this technique well in hand, it should be possible to select a single

crystal, increase its size by crystal growth, and then determine its absolute configuration. This work illustrates the importance of using synergistically different solid state experimental techniques, such as NMR, IR, Raman and VCD, combined with quantum chemical calculations for the elucidation of the structures and the chirality, including the absolute configurations, of crystalline supramolecular organizations. X-ray crystallography on a single crystal is very efficient but does not represent statistical distributions.

ii) VCD is clearly superior to CD[67] for determination of the absolute configuration of conglomerates because it has many more bands to differentiate enantiomers and because vibrational spectra (frequencies and intensities) are much easier to calculate than electronic spectra.[68]

iii) It is important to understand that the VCD experiments only determine that one enantiomer predominates but not the enantiomeric excess (the minor enantiomer cancels the equivalent amount of the major enantiomer bands and those observed corresponds to the excess of the major one).

iv) In a given crystallization experiment and although both enantiomers are equiprobable being of the same energy, there is always one enantiomer more abundant than the other due to many factors (chiral impurity, glass defects, Ostwald ripening,[69] etc.). Therefore, the present results do not mean that the *M/P* predominance could not been inverted in other crystallizations. However, it has been reported several examples of repeated crystallizations starting from an achiral compound yielding always the same enantiomer.[70,71,72,73,74]

v) The characterization of the absolute configuration of the three perfluorinated indazoles by VCD will allow to determine what enantiomer was formed in future experiments, for instance, growing them on chiral surfaces.

Acknowledgements

This work was carried out with financial support from the Ministerio de Economía y Competitividad (Project Nos. CTQ2014-56833R and CTQ2015-63997-C2-2-P), CICE/Junta de Andalucía (P08-FQM-04096) and CICE/JA-FEDER-UJA:Plan de Fortalecimiento de las Capacidades de I+D+i/2014-15 (UJA2013/08/03) and Comunidad Autónoma de Madrid (Project FOTOCARBON, ref. S2013/MIT-2841). Computer, storage and other resources from the CTI (CSIC) are gratefully acknowledged. Authors thank the University of Jaén for continuing financial support, for bridge projects (UJA2015/08/07) and (UJA2016/08/15) and for Acción 2: Financiación de Incentivos a la Excelencia de I+D+i de la UJA 2014-15 in 2014 and 2015 calls and to its CICT for instrumental facilities. M.M.Q.M. thanks the University of Jaén for a pre-doctoral fellowship. The CNRS is acknowledged for support.

References

1 J. Elguero, A. Fruchier and R. Jacquier, *Bull. Soc. Chim. Fr*., 1966, 3041–3042.
2 J. Elguero and R. Wolf, *Comp. Rend. Acad. Sci. Paris*, 1967, **265C**, 1507–1510.
3 J. Elguero, R. Rivière-Baudet and J. Satgé, *Comp. Rend. Acad. Sci. Paris*, 1968, **266C**, 44–47.
4 J. R. Avilés Moreno, M. M. Quesada Moreno, J. J. López González, R. M. Claramunt, C. López, I. Alkorta and J. Elguero, *Chem. Phys. Chem*., 2013, **14**, 3355–3360.
5 I. Alkorta, F. P. Cossío, J. Elguero, N. Fresno, L. Hernández-Folgado, S. García-Granda, L. Menéndez-Taboada, R. Pérez-Fernández, F. Reviriego and L. Vázquez-Viñuela, *New J. Chem*., 2013, **37**, 2384–2398.
6 M. Calafell, J. Elguero and A. Fruchier, *Org. Magn. Reson*., 1975, **7**, 84–85.
7 C. Fernández-Castaño, C. Foces-Foces, F. H. Cano, R. M. Claramunt, C. Escolástico, A. Fruchier and J. Elguero, *New J. Chem*., 1997, **21**, 195–213.
8 M. S. Rodríguez-Morgade, C. G. Claessens, A. Medina, D. González-Rodríguez, E. Gutiérrez-Puebla, A. Monge, I. Alkorta, J. Elguero and T. Torres, *Chem. Eur. J*., 2008, **14**, 1342–1350.

9 M. Pérez-Torralba, M. Á. García, C. López, M. C. Torralba, M. R. Torres, R. M. Claramunt and J. Elguero, *Cryst. Growth Des*., 2014, **14**, 3499–3509.
10 C. I. Nieto, M. P. Cabildo, M. P. Cornago, D. Sanz, R. M. Claramunt, M. C. Torralba, M. R. Torres, J. Elguero, J. A. García, A. López and D. Acuña-Castroviejo, *Molecules*, 2015, **20**, 15643–15665.
11 J. Teichert, P. Oulié, K. Jacob, L. Vendier, M. Etienne, R. M. Claramunt, C. López, C. Pérez Medina, I. Alkorta and J. Elguero, *New J. Chem*., 2007, **31**, 936–946.
12 R. M. Claramunt, C. López, C. Pérez-Medina, M. Pérez-Torralba, J. Elguero, G. Escames and D. Acuña-Castroviejo, *Bioorg. Med. Chem*., 2009, **17**, 6180–6187.
13 R. M. Claramunt, C. López, A. López, C. Pérez-Medina, M. Pérez-Torralba, I. Alkorta, J. Elguero, G. Escames and D. Acuña-Castroviejo, *Eur. J. Med. Chem*., 2011, **46**, 1439–1447.
14 C. Pérez Medina, C. López, R. M. Claramunt and J. Elguero, *J. Heterocycl. Chem*., 2009, **46**, 1408–1412.
15 A. Caballero, E. Despagnet-Ayoub, M. M. Díaz-Requejo, A. Díaz-Rodríguez, M. E. González-Núñez, R. Mello, B. K. Muñoz, W.-S. Ojo, G. Asensio, M. Etienne and P. J. Pérez, *Science*, 2011, **332**, 835–838.
16 W.-S. Ojo, K. Jacob, E. Despagnet-Ayoub, B. K. Muñoz, S. Gonell, L. Vendier, V.-H. Nguyen and M. Etienne, *Inorg. Chem*., 2012, **51**, 2893–2901.
17 C. Pérez-Medina, C. López, M. P. Cabildo, R. M. Claramunt, M. C. Torralba, M. R. Torres, I. Alkorta and J. Elguero, *J. Mol. Struct*., 2012, **1022**, 139–146.
18 M. Á. Fuentes, B. K. Muñoz, K. Jacob, L. Vendier, A. Caballero, M. Etienne and P. J. Pérez, *Chem. Eur. J*., 2013, **19**, 1327–1334.
19 B. K. Muñoz, W.-S. Ojo, K. Jacob, N. Romero, L. Vendier, E. Despagnet-Ayoub and M. Etienne, *New J. Chem*., 2014, **38**, 2451–2461.
20 N. Romero, S.-C. Rosca, Y. Sarazin, J.-F. Carpentier, L. Vendier, S. Mallet-Ladeira, C. Dinoi and M. Etienne, *Chem. Eur. J*., 2015, **21**, 4115–4125.
21 Y.-K. Lee, D. J. Parks, T. Lu, T. V. Thieu, T. Markotan, W. Pan, D. F. McComsey, K. L. Milkiewicz, C. S. Crysler, N. Ninan, M. C. Abad, E. C. Giardino, B. E. Maryanoff, B. P. Damiano and M. R. Player, *J. Med. Chem*., 2008, **51**, 282–297.
22 S. Fustero, A. Simón-Fuentes, O. Delgado and R. Román. Fluorinated Pyrazoles and Indazoles (see page 309), in V. Nenajdenko, Ed. "Fluorine in Heterocyclic Chemistry, Vol. 1, Springer, Switzerland, 2014.
23 J. Magano, M. Waldo, D. Greene and E. Nord, *Org. Proc. Res. Develop*., 2008, **12**, 877–883.
24 M. Andersson, X. Diao, A. Wohlfarth, K. B. Scheidweiler and M. A. Huestis, *Rapid Commun. Mass Spectrom*., 2016, **30**, 1067–1078.
25 Neuropathology of Drug Addictions and Substance Misuse, Vol. 2, V. R. Preedy, Ed., Academic Press, London, 2016.
26 J. Hu, H. Xu, P. Nie, X. Xie, Z. Nie and Y. Rao, *Chem. Eur. J*., 2014, **20**, 3932–3938.
27 L. Sun, J. Nie, Y. Zheng and J.-A. Ma, *J. Fluor. Chem*., 2015, **174**, 88–94.
28 B. A. Hathaway, G. Day, M. Lewis and R. Glaser, *J. Chem. Soc., Perkin Trans. 2*, 1998, 2713–2719.
29 E. Escande, J. Lapasset, R. Faure, E. J. Vincent and J. Elguero, *Tetrahedron*, 1974, **30**, 2903–2909.
30 J. Elguero, I. Alkorta, R. M. Claramunt, P. Cabildo, P. Cornago, M. Á. Farrán, M. Á. García, C. López, M. Pérez-Torralba, D. Santa María and D. Sanz, *Chem. Heterocycl. Comp*., 2013, 177–202.
31 C. Foces-Foces, *Acta Crystallogr., Sect. E*, 2005, **61**, o337–o339.
32 J. Jacques, A. Collet and S. H. Wilen, Enantiomers, Racemates and Resolutions, Kriger Publishing Co, Malabar, Florida, 1994.
33 R. M. Tejedor, S. Uriel, S. Graus, T. Sierra, J. L. Serrano, R. M. Claramunt, C. López, M. Pérez-Torralba, I. Alkorta and J. Elguero, *Chem. Eur. J*., 2013, **19**, 6044–6051.

34 J. J. L. González, F. P. Ureña, J. R. A. Moreno, I. Mata, E. Molins, R. M. Claramunt, C. López, I. Alkorta and J. Elguero, *New J. Chem*., 2012, **36**, 749–758.
35 A. G. Cairns-Smith, Seven Clues to the Origin of Life, Cambridge University Press, Cambridge, 1985.
36 A. Guijarro, M. Yus, The Origin of Chirality in the Molecules of Life, RSC, Cambridge, 2009.
37 L. Pérez-García, D. B. Amabilino, *Chem. Soc. Rev.* 2002, **31**, 342–356.
38 J. S. Siegel, *Chirality* 1998, **10**, 24–27.
39 P. Cabildo, R. M. Claramunt, F. J. Zúñiga, I. Alkorta and J. Elguero, *Z. Kristallogr*., 2015, **230**, 427–438.
40 A. Escande, J. L. Galigné and J. Lapasset, *Acta Crystallogr., Sect. B*, 1974, **30**, 1490–1495.
41 P. D. Du Bois Murphy, *J. Magn. Reson*., 1983, **52**, 343–345.
42 P. D. Du Bois Murphy, *J. Magn. Reson*., 1985, **62**, 303–308.
43 L. B. Alemany, D. M. Grant, T. D. Alger and R. J. Pugmire, *J. Am. Chem. Soc*., 1983, **105**, 6697–6704.
44 R. Kuroda, T. Harada and Y. Shindo, *Rev. Sci. Instrum.,* 2001, **72**, 3802–3810.
45 C. Merten, T. Kowalik and A. Hartwig, *Appl. Spectrosc.*, 2008, **62**, 901–905.
46 T. Buffeteau, F. Lagugné-Labarthet and C. Sourisseau, *Appl. Spectrosc.*, 2005, **59**, 732−745.
47 P. A. Hariharan and J. A. Pople, *Theor. Chim. Acta*, 1973, **28**, 213–222.
48 M. J. Frisch, J. A. Pople and J. S. Binkley, *J. Chem. Phys*., 1984, **80**, 3265–3269
49 R. Ditchfield, *Mol. Phys*., 1974, **27**, 789–807.
50 F. London, *J. Phys. Radium*., 1937, 8397–409.
51 M. J. Frisch, G. W. Trucks, H. B. Schlegel, G. E. Scuseria, M. A. Robb, J. R. Cheeseman, G. Scalmani, V. Barone, B. Mennucci, G. A. Petersson, H. Nakatsuji, M. Caricato, X. Li, H. P. Hratchian, A. F. Izmaylov, J. Bloino, G. Zheng, J. L. Sonnenberg, M. Hada, M. Ehara, K. Toyota, R. Fukuda, J. Hasegawa, M. Ishida, T. Nakajima, Y. Honda, O. Kitao, H. Nakai, T. Vreven, J. A. Montgomery, Jr., J. E. Peralta, F. Ogliaro, M. Bearpark, J. J. Heyd, E. Brothers, K. N. Kudin, V. N. Staroverov, R. Kobayashi, J. Normand, K. Raghavachari, A. Rendell, J. C. Burant, S. S. Iyengar, J. Tomasi, M. Cossi, N. Rega, J. M. Millam, M. Klene, J. E. Knox, J. B. Cross, V. Bakken, C. Adamo, J. Jaramillo, R. Gomperts, R. E. Stratmann, O. Yazyev, A. J. Austin, R. Cammi, C. Pomelli, J. W. Ochterski, R. L. Martin, K. Morokuma, V. G. Zakrzewski, G. A. Voth, P. Salvador, J. J. Dannenberg, S. Dapprich, A. D. Daniels, Ö. Farkas, J. B. Foresman, J. V. Ortiz, J. Cioslowski and D. J. Fox, Gaussian 09, Revision D.01, Gaussian, Inc., Wallingford CT, 2009.
52 A. M. S. Silva, R. M. S. Sousa, M. L. Jimeno, F. Blanco, I. Alkorta and J. Elguero, *Magn. Reson. Chem*., 2008, **46**, 859–864.
53 F. Blanco, I. Alkorta and J. Elguero, *Magn. Reson. Chem*., 2007, **45**, 797–800.
54 N. Fresno, R. Pérez-Fernández, M. L. Jimeno, I. Alkorta, G. Sánchez-Sanz, J. Elguero and J. E. Del Bene, *J. Heterocycl. Chem*., 2012, **49**, 1257–1259.
55 SIR92 - A program for crystal structure solution. A. Altomare, G. Cascarano, C. Giacovazzo and A. Guagliardi, *J. Appl. Cryst.*, 1993, **26**, 343–350.
56 SHELX97 [Includes SHELXS97, SHELXL97, CIFTAB] - Programs for Crystal Structure Analysis (Release 97-2). G. M. Sheldrick, Institüt für Anorganische Chemie der Universität, Tammanstrasse 4, D-3400 Göttingen, Germany, 1998.
57 WINGX - 1.63 Integrated System of Windows Programs for the Solution, Refinement and Analysis of Single Crystal X-Ray Diffraction Data. L. Farrugia, *J. Appl. Cryst.*, 1999, **32**, 837–838.
58 CRYSTALS version 12: software for guided crystal structure analysis . P. W. Betteridge, J. R. Carruthers, R. I. Cooper, K. Prout and D. J. Watkin, *J. Appl. Crystallogr.*, 2003, **36**, 1487.
59 International Tables for X-Ray crystallography, 1974, Vol IV, Kynoch press, Birmingham, England.

60 H. D. Flack, *Acta Cryst.* 1983, A**39**, 876–881.
61 R. W. W. Hooft, L. H. Straver and A. L. Spek, *J. Appl. Crystallogr.*, 2008, **41**, 96-103.
62 NIST Standard Reference Database 101; Computational Chemistry Comparison and Benchmark Database: http://cccbdb.nist.gov/.
63 P. J. Stephens, F. J. Devlin and J. R. Cheeseman, VCD Spectroscopy for Organic Chemists, CRC Press, Boca Raton, 2012.
64 P. J. Stephens, F. J. Devlin, C. F. Chabalowski and M. J. Frisch, *J. Phys. Chem.*, 1994, **98**, 11623-11627.
65 P. J. Stephens, F. J. Devlin and J.-J. Pan, *Chirality*, 2008, **20**, 643-663.
66 M. M. Quesada-Moreno, J. R. Avilés-Moreno, J. J. López-González, R. M. Claramunt, C. López, I. Alkorta and J. Elguero, *Tetrahedron Asymm.*, 2014, **25**, 507–515.
67 D. T. McLaughlin, T. P. T. Nguyen, L. Mengnjo, C. Bian, Y. H. Leung, E. Goodfellow, P. Ramrup, S. Woo and L. A. Cuccia, *Cryst. Growth. Des.*, 2014, **14**, 1067–1076.
68 Handbook of Molecular Biophysics: Methods and Applications, H. G. Bohr, Ed., Wiley-VCH, Weinheim, 2009.
69 T. Vetter, M. Iggland, D. R. Ochsenbein, F. S. Hänseler and M. Mazzotti, *Cryst. Growth. Des.*, 2013, **13**, 4890–4905.
70 P. S. M. Cheung, J. Gagnon, J. Surprenant, Y. Tao, H. Xu and L. A. Cuccia, *Chem. Commun.*, 2008, 987–989.
71 S. Azeroual, J. Surprenant, T. D. Lazzara, M. Kocun, Y. Tao, L. A. Cuccia and J.-M. Lehn, *Chem. Commun.*, 2012, **48**, 2292–2294.
72 K. Ziach and J. Jurczak, *Chem. Commun.*, 2015, **51**, 4306–4309.
73 A. Lennartson and M. Håkansson, *New J. Chem.*, 2015, **39**, 5936–5943.
74 C.-Y. Gao, F. Wang, H.-R. Tian, L.-J. Li, J. Zhang and Z.-M. Sun, *Inorg. Chem.*, 2016, **55**, 537–539.